DIII-D Experimental Simulation of ITER Scenario Access and Termination

G.L. Jackson[1], P.A. Politzer[1], D.A. Humphreys[1], T.A. Casper[2], A.W. Hyatt[1], J.A. Leuer[1], J. Lohr[1], T.C. Luce[1], M.A. Van Zeeland[1], and J.H. Yu[3]

[1]General Atomics, P.O. Box 85608, San Diego, California 92186-5608, USA
[2]ITER Organization, Route de Vinon sur Verdon, F-13115 Saint Paul lez Durance, France
[3]University of California-San Diego, 9500 Gilman Dr., La Jolla, California 92093, USA

e-mail: jackson@fusion.gat.com

Abstract. Reliable access to and termination of burning plasma scenarios is crucial for the success of the ITER mission. DIII-D has simulated both the startup and rampdown phases by scaling the ITER shape and plasma current penetration time to DIII-D experimental conditions. Both improved ramp-up and rampdown scenarios have been developed by experimentally simulating ITER conditions and operating space has been explored with a variety of scans including a resonant radius scan for electron cyclotron (EC) startup and an initial vertical field scan to optimize EC breakdown. Complete ITER discharges have been experimentally simulated, both for the 15 MA baseline H-mode and 17 MA high fusion yield scenarios including successful rampdown to a "soft landing". Details of the breakdown and initial toroidal current formation have been studied including noninductive plasma currents up to 33 kA during the pre-ionization phase. Benchmarking of these DIII-D discharges using a variety of codes will allow predictive modeling for extrapolation to ITER.

1. Introduction

Reliable access to and termination of burning plasma scenarios is crucial for the success of the ITER mission. DIII-D has simulated both the startup and rampdown phases by scaling the ITER shape and plasma current penetration time to DIII-D experimental conditions [1], We have investigated the discharge evolution both to reach plasma current flattop and to ramp down the discharge to sufficiently low stored magnetic energy and plasma current where an abrupt subsequent termination does not lead to adverse effects such as erosion of plasma facing components (PFCs) or compromising the mechanical integrity of the ITER vessel. With electron cyclotron (EC) assist, startup at low toroidal electric fields expected for ITER ($E_\phi \leq 0.3$ V/m) is robust even when limiting on the low field side (LFS). A complete experimental simulation is shown in Fig. 1 where the discharge is Ohmically ramped to current flattop equivalent to 15 MA in ITER, H-mode (ITER baseline scenario) is achieved at $q_{95} \approx 3$ (flattop duration is not scaled), and rampdown is well controlled, all consistent with ITER specifications scaled to DIII-D. The end of the rampdown phase scales to 1.0 MA in ITER, below the ITER specified value (1.4 MA) for a "soft landing". The control system maintains the strike points nearly fixed, corresponding to the divertor region in ITER while the discharge elongation is continuously reduced to maintain vertical stability using the ITER-prescribed rampdown scenario.

For several years, DIII-D has carried out detailed studies of both the startup and ramp-down of ITER-like conditions by scaling parameters from ITER to DIII-D [1–4], and the work presented here is an extension of these studies. In this paper, we define startup as the phase from breakdown through the plasma current ramp to the programmed I_p flattop value. Experimental studies of ITER-like conditions have been carried out in a variety of tokamaks [5], but the discussion presented here will focus upon DIII-D results. The limiter phase of the current ramp is scaled by the ratio of the LFS major radii of both devices, $R_{LFS,ITER}/R_{LFS,DIII\text{-}D} \approx 3.5$. This scaling was chosen because the initial ITER startup scenario envisaged a LFS field null and breakdown [6]. The more recent startup scenarios, used in this paper, include a central large-bore startup with the same major radii [3,4]. During the later diverted phases, a scaling factor of 3.65 was determined by the ITER flattop equilibrium target. The

DIII-D toroidal field used in this work, B_T, was 1.9–2.1 T at the major radius R = 1.7 m (compared to 5.3 T at R = 6.2 m in ITER). Based on gyro-Bohm scaling ($T_e \propto B_T^{2/3} a^{1/3}$), the ratio between the current redistribution time in ITER and DIII-D is about 50 (a is the minor radius). Since dimensions and toroidal fields are specified, the plasma current is determined by requiring the same normalized current, $I_N = I_p/aB_T$, in both devices. For the 15 MA ITER scenario, $I_N = 1.42$ and $q_{95} \approx 3$.

In this paper we discuss studies on plasma initiation, current channel formation and ramp-up (Sec. 2), I_p rampdown (Sec. 3), modeling and benchmarking of these ITER-like discharges (Sec. 4), followed by conclusions.

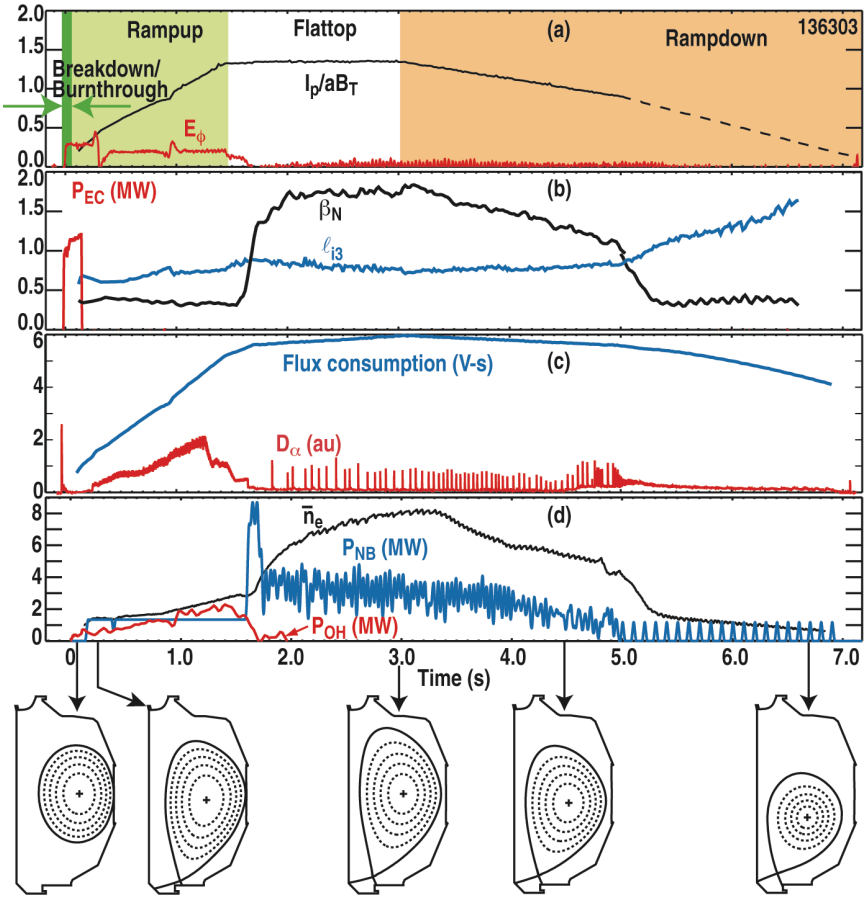

FIG. 1. DIII-D experimental simulation of an ITER (baseline scenario) H-mode discharge (from [1]): (a) 4 phases are shown in different colors with E_ϕ and normalized I_p plotted, (b) EC power, internal inductance, and normalized β, (c) flux consumption and divertor D_α intensity, and (d) Ohmic (red), NB (blue), heating power and line averaged electron density. Dashed line (a) represents the rampdown L-mode phase.

2. Startup

As shown in Fig. 1, startup can be divided into an initial phase (containing breakdown, I_p formation, and burnthrough) and I_p rampup, and these topics are discussed below.

2.1 Breakdown, I_p Formation, and Burnthrough

Since the maximum specified toroidal electric field in ITER, 0.3 V/m, is much lower than most present day tokamaks, EC assist has been proposed to provide an additional margin for successful breakdown and burnthrough [6]. For ITER design parameters the EC fundamental resonant radius (170 GHz), R_{O1} = 5.4 m (R_0^{ITER} = 6.2 m) [7]. However operation of ITER at lower values of B_T will move the resonant radius further inboard, so a resonant radius scan has been carried out in DIII-D (Fig. 2). Discharge shapes were similar [Fig. 2(a)] and EC assisted breakdown was effective at all radii tested [Fig. 2(c)], although a delay in I_p initiation was observed as R_{X2} was decreased [Fig. 2(b)]. As expected, peak electron temperature occurred near the resonant radius [Fig. 2(d)] in all cases.

Plasma breakdown and burnthrough using EC assist are more effective with the addition of a programmed vertical field, $B_{z,pgm}$ in the pre-ionization phase (Fig. 3). Pre-ionization is defined as the time from application of EC heating until E_ϕ is applied (typically at t = -8 ms in

DIII-D). This might seem counter-intuitive since the field null region is significantly reduced as the magnitude of the vertical field is increased (the maximum connection length for a field line to intersect the wall decreases hence the avalanche is less likely), but breakdown and burnthrough are prompt and reproducible and the initial rate of I_p rise is increased. A good field null is required for Ohmic startup alone, but EC assist alters this requirement [8]. Thus best startup conditions with EC assist are different than for the usual tokamak Ohmic startup and this will be an important consideration when EC assist is used in ITER. With 1–1.2 MW of EC assist in these DIII-D experiments, the relevance of a field null, and its location, does not seem to be important.

Both the pre-ionization density [Fig. 3(a)] and initial I_p ramp rate, inferred from [Fig. 3(b)] are lower for helium, but reliable startup was still obtained. A comparison of radial and oblique launch in Fig. 3 shows only small differences if programmed vertical field is optimized. Discharges without EC assist (solid squares) with E_ϕ = 0.3 V/m did not achieve burnthrough [Fig. 3(b)].

During the discharge formation phase the calculated flux derived from the JFIT code, at 3 times is shown in Fig. 4: before closed flux surfaces form [Fig. 4(a)], near the time when closed flux surfaces are first observed [Fig. 4(b)], and later when the discharge is well established, limited on the high field side (HFS) [Fig. 4(c)]. The JFIT reconstruction first solves for toroidal I_p on a specified grid [Fig. 4(d-f)] and then calculates the flux from this reconstruction [9]. For this analysis JFIT can then determine current densities of arbitrary distribution rather than fitting a prescribed current profile (e.g. EFIT) and as such it is especially useful in determining the toroidal current on open field lines, e.g. I_{open} in Fig. 4(g). At

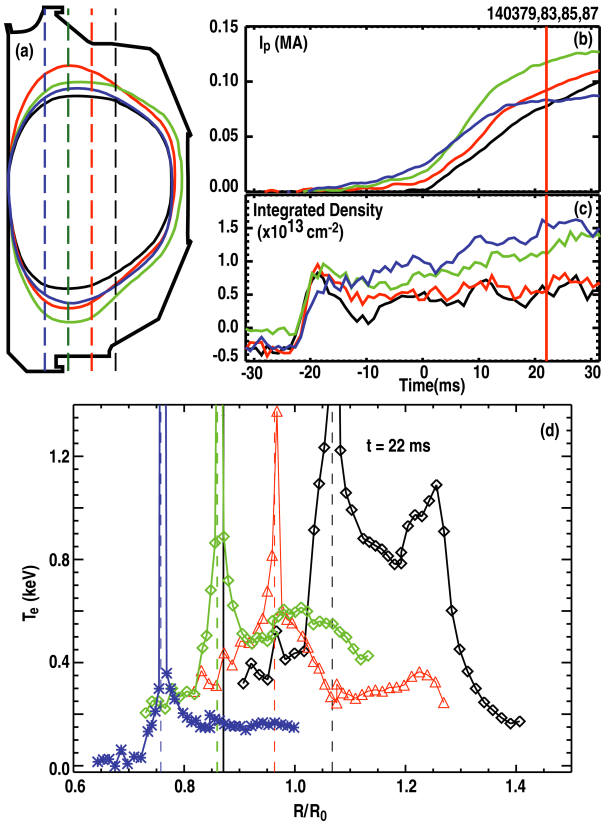

FIG. 2. EC resonant radius scan with 4 discharges at different B_T, (a) plasma shapes at 22 ms and DIII-D outline for plasma facing surfaces, (b) I_p, (c) midplane line integrated density and (d) T_e profile (t = 22 ms) from the ECE radiometer. Dashed vertical lines indicate the EC resonance, R_{X2} (a,d) and the solid vertical line (d) shows the ITER resonance location, R_{O1} for the 170 GHz gyrotrons in the ITER geometry. E_ϕ = 0.3 V/m, $R_{0,DIII\text{-}D}$ = 1.7 m.

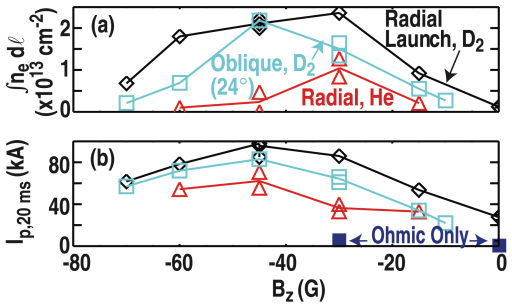

FIG. 3. Maximum line integrated density, (a), during the pre-ionization phase (E_ϕ = 0), and (b) plasma current measured during the early discharge evolution at t = 20 ms as a function of initial applied vertical field. P_{EC} = 1-1.2 MW (2nd harmonic), either radial or oblique (24°) launch, E_ϕ = 0.3 V/m, and B_ϕ = 1.9 T. Two Ohmic attempts (no burnthrough) with similar parameters are also shown (b, solid squares). Helium discharges (radial launch) are shown in red.

t = -4 ms all plasma current is still on open field lines, Fig. 4(a,g). The current inside the last closed flux surface (LCFS) is well defined by t = +4 ms, where I_{LCFS} = 14 kA [Fig. 4(b)]. The current distribution at this tme is shown in Fig. 4(e). Note that significant current density on open field lines is still present. By t = +12 ms (I_{LCFS} = 53 kA), most current is inside the LCFS and the discharge has evolved into a more conventional tokamak equilibria with only a small fraction of the toroidal plasma current on open field lines.

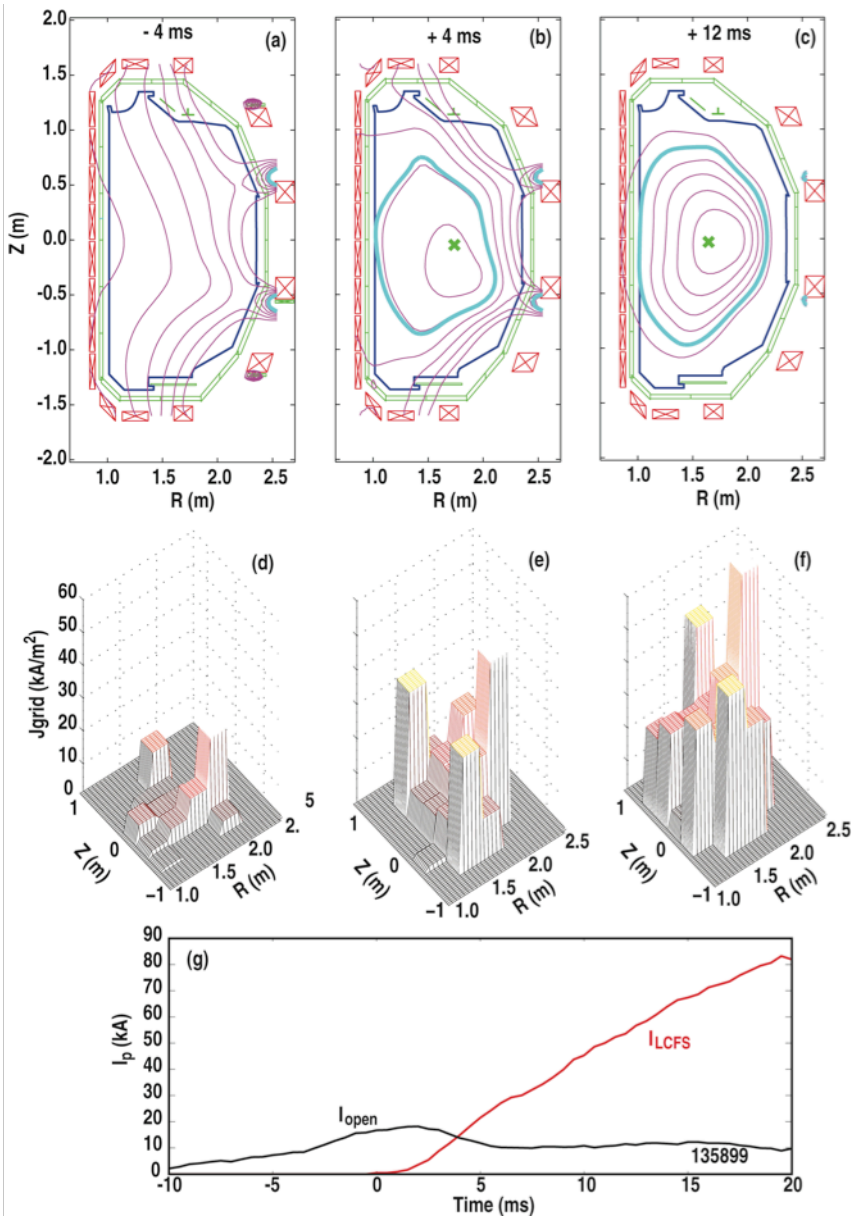

FIG. 4. Flux (a–c) contours and toroidal plasma current density (d–f) for 3 times during breakdown and current formation: -4 ms (a,d), +4 ms (b,e), and +12 ms (c,f). Flux contours are plotted every 0.01 Wb and the LCFS is shown in cyan for (b) and (c). In (g) plasma calculated from JFIT on open field lines is shown as black and inside the LCFS in red.

2.2 Plasma Current Rampup

During the early rampup phase, ITER startup scenarios specify that the discharge will be limited on either the HFS or LFS, diverting later in the ramup sequence (e.g. Fig. 1). In order to reduce the heating of the plasma facing components, a large-bore startup scenario was developed and successfully demonstrated in DIII-D where the plasma was diverted earlier in time (corresponding to $I_{p,divert}$ = 4.5 MA) compared to the original ITER baseline startup scenario ($I_{p,divert}$ = 7.5 MA) [4].

Most of the work reported in this paper has used EC assist and E_ϕ = 0.3 V/m, but Ohmic startup has also been investigated. As reported previously [1,3], successful Ohmic startup when initially limited on the LFS could only be achieved for $E_\phi \geq$ 0.41 V/m. However in recent experiments limited on the HFS, Ohmic startup at the ITER specified electric field of 0.3 V/m has been demonstrated, although this startup scenario is not as robust as with EC assist. The primary benefit of EC assist is the additional heating power available to burn through the charge states of low Z impurities, relaxing the requirements for inductive Ohmic

heating. For example in DIII-D a comparison of similar discharges showed that the burnthrough time required for O^{+4} decreased from 47 ms to 12 ms with EC assist [1].

Methods to reduce flux consumption are important for ITER, in order to have sufficient flux for the specified burn time. The previous discussion presented results for EC assist during breakdown and burnthrough, but flux during the rampup phase can be reduced by the addition of modest amounts of auxiliary heating. A comparison of flux consumption with Ohmic heating to discharges with neutral beam (NB) heating or EC heating shows that the auxiliary heated discharges exhibited an ≈20% reduction in flux required to reach current flattop [1]. Although the temporal trajectories of $l_i(3)$ were different, all three discharges had approximately the same value of internal inductance at current flattop implying the reduction is in the resistive flux consumption. In this comparison, the average heating power for the Ohmic discharge during the I_p rampup was 1.5 MW, compared to total input power of 2.6 MW for the NB case and 2.4 MW for the EC case. For these two auxiliary heated discharges, the Ohmic input contribution was 1.3 MW, so roughly half of the average input power was due to auxiliary heating.

2.3 Noninductive I_p Initiation

In Fig. 4(g), a small plasma current is measured during the noninductive phase ($t \le$ -8 ms). Although the maximum noninductive current has not been optimized, pre-ionization currents as high as 33 kA in other discharges have been measured and an example is shown in Fig. 5. To our knowledge this is the highest current yet obtained for this type of plasma, and is an extension of the work in DIII-D reported in Ref. [10]. These values of I_p may provide a sufficient target for NB or EC current drive and thus open the possibility of a complete noninductive current ramp in future burning plasma devices.

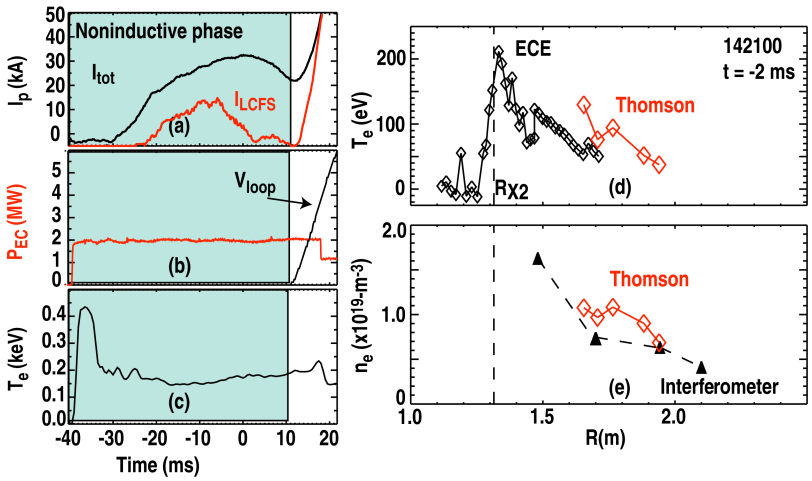

FIG. 5. Up to 33 kA of noninductive plasma current has been measured. Total I_p (I_{tot}) and I_p inside the LCFS (I_{LCFS}) are shown in (a), P_{EC} and V_{loop} in (b), T_e from the ECE radiometer in (c) and profiles of T_e and n_e are plotted in (d) and (e) respectively.

For the discharge in Fig. 5, the start of the inductive phase was delayed to provide a longer pre-ionization phase. The programmed vertical field was decreased (more negative) from -50 to -116 G (-25 ≤ t ≤ 0 ms) to limit on the HFS at higher I_p, then from 0 ≤ t ≤ 10 ms the magnitude was reduced (toward zero) until the inductive startup was enabled at t = +10 ms. In this case closed flux surfaces, indicating a confined plasma during the noninductive phase, were calculated by JFIT and the current inside the LCFS, I_{LCFS}, is shown in Fig. 5(a). The electron temperature profile at the midplane during this noninductive phase, measured by the ECE radiometer and Thomson scattering is shown in Fig. 5(d) and the density profile determined from the IR interferometer and Thomson scattering is plotted in Fig. 5(e). The average interferometer density (solid triangles) is shown, where $\langle n_e \rangle = \int n_e dl / L_{IR}$, and L_{IR} is the total path length inside the vacuum vessel for each interferometer chord. The close agreement between $\langle n_e \rangle$ and $n_{TS}(R)$ implies

that the pre-ionization plasma, at least at the time when the Thomson measurement was available, fills the vacuum vessel.

As discussed in Ref. [11], current on open field lines can be attributed to Pfirsch-Schlüter currents, while the confined plasma current, I_{LCFS} in Figs. 4(g) and 5(a), is due to bootstrap currents. Although modeling of the noninductive phase has not been carried out (EFIT equilibria are not converged during this time), a dimensional analysis shows that the bootstrap current can account for the measured confined current, consistent with the observations in Ref. [11].

3. Plasma Current Rampdown

With the large stored energy in burning plasma devices such as ITER, safe and controlled termination of these discharges is an important aspect of their operation. ITER has prescribed a rampdown scenario [12], and this has been experimentally simulated in DIII-D. With the scaling described in Sec. 1, DIII-D has closely matched normalized parameters q_{95}, κ, $l_i(3)$, and I_N to the ITER DINA rampdown reference scenario [2]. With this scenario, rampdown to below the ITER specified value, $I_{p,ITER}$ = 1.4 MA ($I_{p,DIII\text{-}D}$ = 0.14 MA) was achieved (e.g. Fig. 1). Although additional flux was not required from the entire poloidal field set during this rampdown, additional current in the central solenoid (CS) and inner poloidal field (PF) coils in DIII-D was required, and this might limit flattop duration in ITER so as to not exceed the current limits of the CS coils. Hence alternate scenarios were investigated with a faster current rampdown. As reported in Ref. [2], a faster rampdown produced conditions where no additional CS or inner PF currents were observed. At the fastest L-mode rampdown rate, however, there was a disruption, indicating a window in current ramp rate for successful rampdown in DIII-D without requiring additional CS current [2].

DIII-D has successfully simulated Ohmic discharges, except for EC assisted breakdown and burnthrough in the first 0.22 s (Fig. 6, black traces). Also shown in Fig. 6 (blue traces) is a discharge to evaluate the ITER high Q (17 MA) scenario. This discharge was successfully terminated below the ITER equivalent 1.4 MA threshold for a "soft landing". The Ohmic (black) and high Q (blue) H-mode discharges are also compared with an H-mode (ITER scenario 2) discharge, Fig. 6 (red). Note that both the Ohmic discharge and the scenario 2 (15 MA ITER equivalent) discharge have essentially the same rampdown characteristics. In the scenario 2 case, the high power phase was terminated during I_p flattop to evaluate the H to L transition and Ohmic rampdown. The H-L transition occurs 0.23 s after P_{NB} is reduced. After a few energy confinement times, ($\tau_E \approx 0.15$ s) the discharge has no "memory" of the previous condition (H-mode or Ohmic

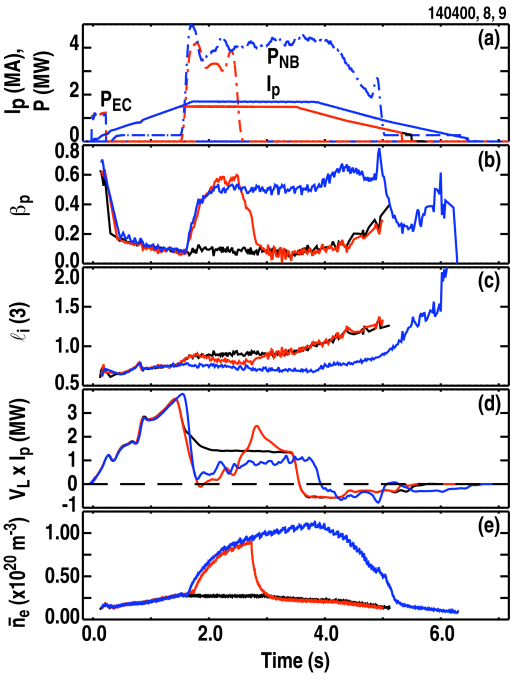

FIG. 6. Parameters for 3 ITER-like discharges, including the rampdown phase. An Ohmic discharge [except for a short EC pulse (a, dashed lines) from -0.015 to 0.225 s] is shown in black and compared to an H-mode discharge (in flattop) in red. A high Q (17 MA ITER equivalent) discharge is plotted in blue. Also plotted are (a) I_p (black and red lines overlap) and neutral beam power (dash-dot), (b) $\beta_{poloidal}$, (c) internal inductance, (d) inductive input power from the Ohmic heating system, and (e) line average electron density.

L-mode). Note also that in both discharges with an H-mode phase there are large ELMs indicated by drops in the electron density [Fig. 6(e)]. These are most pronounced in the high Q (17 MA equivalent) discharge (f_{ELM} = 9 Hz). Since P_{NB} (and therefore H-mode) is programmed to continue into ramp-down for the high Q case, the details of the ramp-down are different than the other two discharges.

In addition to maintaining the strike points fixed during rampdown as the plasma is shifted downward (Fig. 1), vertical stability must also be maintained. In these DIII-D experiments, this has required changing vertical control algorithms during the rampdown, as will likely be the case for ITER also. However, the discharges were still terminated by a vertical displacement event (VDE) disruption, albeit at a low enough current to achieve a "soft landing". In order to benchmark the vertical control and extrapolate to ITER, the DIII-D vertical control system was disabled by freezing all coil current voltage commands just prior to the disruption, and the vertical instability growth rate was measured. This produced a reliable calculation of the closed loop control boundary in terms of controllability metrics. Controllability can be quantified by the maximum vertical displacement metric, ΔZ_{MAX} that a plasma can be displaced suddenly and still be controlled [13]. Previous experiments on DIII-D have shown that a value of ΔZ_{MAX} = 2.5 cm corresponds to marginal control robustness, with the possibility of a VDE. The data in these experiments were consistent with the previous observations [1,14].

The ΔZ_{MAX} normalized by minor radius, $\Delta Z_{MAX}/a$, represents a machine-independent specification of performance used to guide the design of new in-vessel coils for ITER. The vertical stability control system used in these DIII-D experiments simulating ITER rampdown employed only the outboard PF coils, with similar $\Delta Z_{MAX}/a$ to that provided by the ITER in-vessel coils [~10% for the ITER target shape at $l_i(3)$=1.1]. If the dominant source of noise in ITER scales with minor radius and plasma current (typical of power supply or plasma-sourced noise, but not instrumentation noise), these experiments imply that ITER may also experience such a rampdown-terminating VDE, but well below the maximum ITER current level specified as an acceptable "soft landing" (1.4 MA).

4. Modeling and Benchmarking ITER-like Discharges in DIII-D

In order to extrapolate the DIII-D experiments to ITER, benchmarking of these discharges using physics based models is necessary. The Corsica free boundary equilibrium code, TRANSP, and ONETWO have all been used to benchmark these DIII-D discharges with the eventual goal of providing predictive modeling for ITER. Corsica modeling predicts the approximate time of sawteeth onset (q_{min}=1) and reproduces electron temperature evolution during the startup phase. Details of the current profile and internal inductance have been shown to be sensitive to the conductivity in the outer portion of the discharge [15].

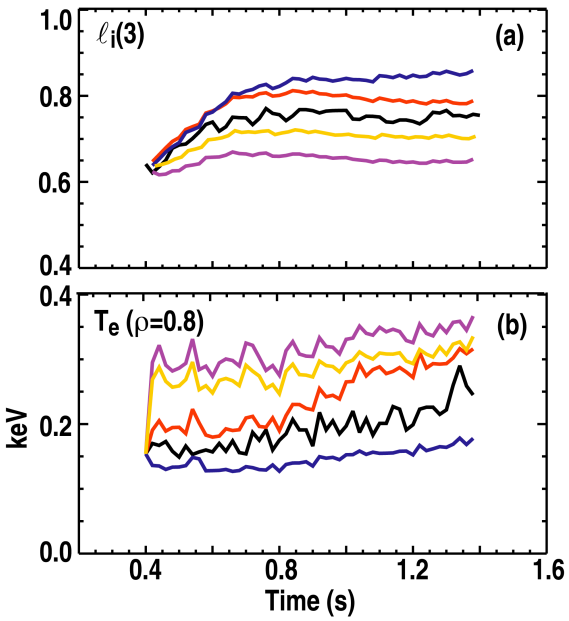

Fig. 7. Calculated time evolution, initialized at t = 0.4 s, for (a) $l_i(3)$ and (b) $T_e(\rho=0.8)$ using 4 transport models: MMM95(red), Bohm/gyroBohm (blue), GLF23 (purple) and TGLF (yellow). Experimental data (#132411) is shown for comparison (black).

Recent transport analysis of ITER-similar current rampup discharges in DIII-D at different values of $l_i(3)$ and type of heating has been carried out to identify the dominant transport mechanism in L-mode discharges during I_p rampup. For the initial analysis, simulations with various transport models, namely TGLF [16], GLF23 [17], MMM95 [18], and Bohm/gyroBohm [19], have been directly compared with experiment. An example is shown in Fig. 7(a) where there is a range of variation in the predicted $l_i(3)$ in the different models, primarily resulting from inaccuracy of the calculated T_e profile in outer radius region ($\rho > 0.7$), as discussed in Ref. [15]. This is also reflected in the calculated time evolution of the electron temperature at $\rho=0.8$ [Fig. 7(b)]. We emphasize that these are the first attempts at comparing the various transport models with DIII-D data and they will be further refined in future work.

As discussed in Sec. 3, normalized parameters have been matched to DINA modeling of ITER for the rampdown phase, but predictive modeling of this phase has not yet been carried out.

5. Conclusions

In DIII-D, experimental simulations of complete of ITER discharges have been achieved, including breakdown, rampup, ITER flattop scenario 2 H-mode, and rampdown with a "soft landing". In experiments reported previously, hybrid discharges have also been obtained using the ITER large-bore startup scenario [3]. Complete Ohmic (possibly required in the ITER commissioning phase) and high Q (17 MA ITER equivalent) discharges have also been demonstrated. Modest amounts of EC power (≈1 MW) during the breakdown and burnthrough phases have been shown to allow robust and reproducible startup with the ITER specified inductive electric fields (0.3 V/m), over a range of toroidal fields, oblique EC launch angles, and EC resonant radii, showing that EC assist is possible in ITER at reduced toroidal field. Noninductive plasmas, up to 33 kA, have also been obtained with EC and this may provide a target for noninductive auxiliary heated current ramp-up. These experiments show that access to ITER flattop scenarios, and successful termination should be possible under a variety of conditions in ITER.

This work was supported in part by the US Department of Energy under DE-FC02-04ER54698 and DE-FG02-07ER54917.

References

[1] JACKSON, G.L., et al., Phys. Plasmas **17** (2010) 056116
[2] POLITZER, P.A., et al., Nucl. Fusion **50** (2010) 035011
[3] JACKSON, G.L., et al., Nucl. Fusion **49** (2009) 115027
[4] JACKSON, G.L., et al., Nucl. Fusion **48** (2008) 125002
[5] SIPS, A.C.C., et al., Nucl. Fusion **49** (2009) 85015
[6] GRIBOV, Y., et al., Nucl. Fusion **47** (2007) S385
[7] AYMAR, R., et al., Plasma Phys. Control. Fusion **44** (2002) 519
[8] LLOYD, B., et al., Nucl. Fusion **31** (1991) 2031
[9] HUMPHREYS, D.A. and KELLMAN, A.G., Phys. Plasmas **6** (1999) 2742
[10] FOREST, C.B., et al., Phys. Plasmas **1** (1994) 1568
[11] EJIRI, A., et al., Nucl. Fusion **46** (2006) 709
[12] KAVIN, A.A., et al., Report ITER_D_2FRCJY V1.1 (Dec. 2008).
[13] HUMPHREYS, D.A., Nucl. Fusion **49** (2009) 115003
[14] POLITZER, P.A., Proc. 37th European Physical Society, Dublin, Ireland, June 2010.
[15] CASPER, T.A., et al., "DIII-D Experimental Verification of Model Predictions for ITER Startup Scenarios," submitted to Nucl. Fusion (2010); and Bull. Am. Phys. Soc. **53** (2008) 202
[16] STAEBLER, G.M., et al., Phys. Plasmas 12 (2005) 102508
[17] WALTZ, R.E., et al., Phys. Plasmas **4** (1997) 2482
[18] BATEMAN, G., et al., Phys. Plasmas **5** (1998) 1793
[19] ERBA, M., et al., Nucl. Fusion **38** (1998) 1013